



## LJMU Research Online

Duan, M, Zhang, JF, Ji, Z, Zhang, WD, Kaczer, B and Asenov, A

**Key issues and solutions for characterizing hot carrier aging of nano-meter scale nMOSFETs**

<http://researchonline.ljmu.ac.uk/id/eprint/6204/>

### Article

**Citation** (please note it is advisable to refer to the publisher's version if you intend to cite from this work)

**Duan, M, Zhang, JF, Ji, Z, Zhang, WD, Kaczer, B and Asenov, A (2017) Key issues and solutions for characterizing hot carrier aging of nano-meter scale nMOSFETs. IEEE Transactions on Electron Devices, 64 (6). pp. 2478-2484. ISSN 0018-9383**

LJMU has developed **LJMU Research Online** for users to access the research output of the University more effectively. Copyright © and Moral Rights for the papers on this site are retained by the individual authors and/or other copyright owners. Users may download and/or print one copy of any article(s) in LJMU Research Online to facilitate their private study or for non-commercial research. You may not engage in further distribution of the material or use it for any profit-making activities or any commercial gain.

The version presented here may differ from the published version or from the version of the record. Please see the repository URL above for details on accessing the published version and note that access may require a subscription.

For more information please contact [researchonline@ljmu.ac.uk](mailto:researchonline@ljmu.ac.uk)

<http://researchonline.ljmu.ac.uk/>

# Key issues and solutions for characterizing hot carrier aging of nano-meter scale nMOSFETs

M. Duan, J. F. Zhang, Z. Ji, W. Zhang, B. Kaczer, and A. Asenov

**Abstract**—Silicon bandgap limits the reduction of operation voltage when downscaling device sizes. This increases the electrical field within a device and hot carrier aging (HCA) is becoming an important reliability issue again for some CMOS technologies. For nano-devices, there are a number of challenges for characterizing their HCA: the random charge-discharge of traps in gate dielectric causes ‘within-a-device-fluctuation (WDF)’, making the parameter shift uncertain after a given HCA. This can introduce errors when extracting HCA time exponents and it will be shown that the lower envelope of the WDF must be used. Nano-devices also have substantial device-to-device variation (DDV) and multiple tests are needed for evaluating their standard deviation,  $\sigma$ , and mean value,  $\mu$ . Repeating the time-consuming HCA tests is costly and a voltage-step-stress method is applied to reduce the number of tests by 80%. For a given number of devices under tests (DUTs), there is little information on the accuracy of the extracted  $\sigma$  and  $\mu$ . We will develop a method to provide this information, based on the defect-centric model. For 40 DUTs with an average of 10 traps per device, the extracted  $\mu$  and  $\sigma$  has an accuracy of  $\pm 14\%$  and  $\pm 24\%$  respectively with a 95% confidence.

*Index terms:* Hot carriers, Aging, Device-to-device variations, Time dependent variations, BTI, Random Telegraph Noise, Instabilities, Fluctuation, Reliability, Defects.

## I. INTRODUCTION

In 1980s, hot carrier aging (HCA) was the most important reliability issue as downscaling device size without reducing operation voltage,  $V_{dd}$ , increases electrical field within the device [1]-[3]. HCA was alleviated since 1990s, because of the reduced  $V_{dd}$ . As  $V_{dd}$  approaches the limit imposed by the silicon bandgap, downscaling the channel length leads to a rapid rise of HCA [4]-[6]. It has been reported that, for some CMOS technologies, HCA can even be more severe than bias temperature instabilities [4]-[6] and HCA has been revisited by many researchers recently [4-17]. There are important differences between the HCA of nano-devices and the classical HCA in 1980s. For example, the worst HCA used to occur under  $V_g \sim V_{dd}/2$ , but HCA of nano-devices under

$V_g = V_d = V_{dd}$  is substantially higher than that under  $V_g \sim V_{dd}/2$  [5,9,11]. It is proposed that the HCA of nano-devices is driven by carrier energy and carrier-carrier interaction [11,14,16,17] and multi-vibration excitation [11] play important roles. The objective of this work is to investigate some key issues in characterizing the HCA of nano-nMOSFETs.

The HCA kinetics follows a power law against both stress time and biases [1,18],

$$HCA = C V^m t^n, \quad (1)$$

where  $C$  is a constant. To predict the long term HCA under operation  $V_{dd}$ , it is important to extract the exponent,  $m$  and  $n$ , accurately, but there are a number of challenges for this extraction from nano-devices. In our recent iedm work [5], we addressed two key issues:

(i) In the presence of ‘within-a-device-fluctuation (WDF)’ [19,20] for nano-devices, one must use the lower envelope of the WDF when extracting the time exponent.

(ii) The device-to-device variation (DDV) requires repeating the tests many times to obtain the statistical properties [21,22]. Aging tests are time consuming and its repetition is costly. The voltage step stress technique can reduce the number of tests by 80%.

In this work, in addition to describe the above two issues in more details, we extend the iedm work [5] by addressing another two key issues:

(iii) The accuracy of the evaluated standard deviation,  $\sigma$ , and the mean value,  $\mu$ , of DDV increases with the number of devices under tests (DUTs). In practice, however, the number of DUTs is limited by test time. When a limited number of DUTs is used for evaluating  $\sigma$  and  $\mu$ , there is little information on their accuracy. For the first time, we will develop a method for estimating their accuracy against the number of DUTs.

(iv) During HCA, positive bias temperature instability (PBTI) occurs near the source [12]. The effect of PBTI on the kinetics of HCA will be assessed.

## II. DEVICES AND EXPERIMENTS

The MOSFETs used were fabricated by a 28 nm planar CMOS technology. The channel length and width are  $27 \times 90$  nm with HK/metal gate. A wide channel length of 900 nm was also used, reducing the device-to-device variation to  $< \pm 8\%$ . The gate dielectric stack consists of a Hafnium oxide and a SiON interfacial layer with a 1.2 nm equivalent oxide thickness.

The HCA was carried out under  $V_g = V_d$  at 125 °C, rather than room temperature, as it was reported that HCA increases

Manuscript received MMM DDD, 2016. This work was supported by the Engineering and Physical Science Research Council of UK under the grant no. EP/L010607/1. The test samples were supplied by David Vigar of Cambridge Silicon Radio. The review of this paper was arranged by Editor W. WWW. M. Duan, J. F. Zhang ([J.F.Zhang@ljmu.ac.uk](mailto:J.F.Zhang@ljmu.ac.uk)), Z. Ji, and W. Zhang are with the Department of Electronics and Electrical Engineering, Liverpool John Moores University, Liverpool L3 3AF, U.K.

B. Kaczer is with Imec, Leuven B-3001, Belgium.

A. Asenov is with the Department of Electronics and Electrical Engineering, University of Glasgow, Glasgow G12 8QQ, U.K.

with temperature for modern CMOS nodes [12,23]. The threshold voltage,  $V_{th}$ , was monitored from the  $V_g$  shift under a fixed drain current of  $100 \text{ nA} \times W/L$  [5,24]. The nano-meter devices have an as-fabricated DDV at time zero. Some researchers reported no correlation between the time-zero DDV and time-dependent DDV [22], while others observed a weak correlation [25]. In this work, the effect of this time-zero DDV on the follow-on time-dependent DDV is taken into account by using the time-zero  $I_d$ - $V_g$  of each device as its own reference. For the planar CMOS process used in this work, HCA is more severe for nMOSFETs than for pMOSFETs when stressed under  $|V_g|=V_d$  [11], so that this work will focus on the HCA of nMOSFETs.

Fig. 1(a) shows a typical aging process for a  $27 \times 90 \text{ nm}$  device, where the data were recorded by an oscilloscope at a sampling rate of  $10^6$  points/sec, giving a time resolution of  $1 \mu\text{s}$ , which is fast enough to capture the charge-discharge of traps in gate dielectric [26].

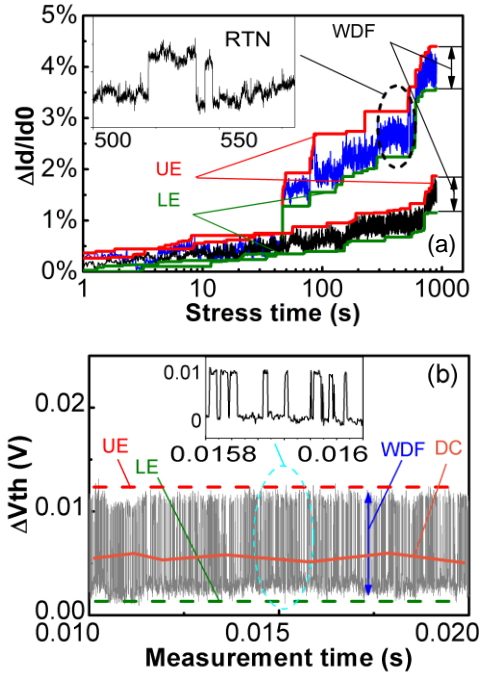


Fig. 1. (a) HCA ( $V_g=V_d=1.3\text{V}$ ) of two  $W=90\text{nm}$  devices shows large DDV. WDF, UE, and LE is ‘within-a-device-fluctuation’, the upper- and the lower-envelope. (b) shows the simplest form of WDF: a two level RTN. The ‘DC’ marked out the average value within 10 ms, as used in a typical SMU.

### III. RESULTS AND DISCUSSIONS

#### A. Extraction of time exponents, $n$

Some typical HCA results are plotted against stress time for two nano-devices in Fig. 1(a). In addition to a substantial DDV, there is a considerable within-a-device-fluctuation (WDF) [19,20]. This fluctuation is not caused by the soft breakdown of the gate dielectric, since the gate current is two orders of magnitude less than the fluctuation in the drain current. Moreover, in its simplest form, the WDF only has two-levels, a signature of random telegraph noise rather than breakdown, and

one example is given in Fig. 1(b). This supports that the fluctuation in Fig. 1(a) originates from the random charge/discharge of traps in gate dielectrics.

The large DDV of WDF in Fig. 1(a) can have two sources: a large variation of trap number per device and a large variation of the impact of one trap on devices. To explain the latter, one should note that the current flow in the device is not uniform [21]. The trap will have a larger impact on a device when the local current beneath it is high [27]. It has been shown that the impact of a trap on the device follows an exponential distribution [21].

The WDF introduces uncertainty to the HCA after a given stress: the parameter shifts can be anywhere between the upper envelope (UE) and lower envelope (LE) of the WDF [19,20]. LE is caused by the defects that do not discharge. Fig. 1(a) shows that LE increases with HCA stress levels, so that these defects were charged by the HC stress. Once they are charged, they remain charged during the measurement. In contrast, ‘UE’ is the upper-envelope of the fluctuation. It contains two components: LE and the fluctuation. It represents the ‘total’ degradation level. When a commercial ‘DC’ source-and-measure unit is used, it effectively takes the average within, for example, 10 ms, as the ‘DC’ line marked out in Fig. 1(b).

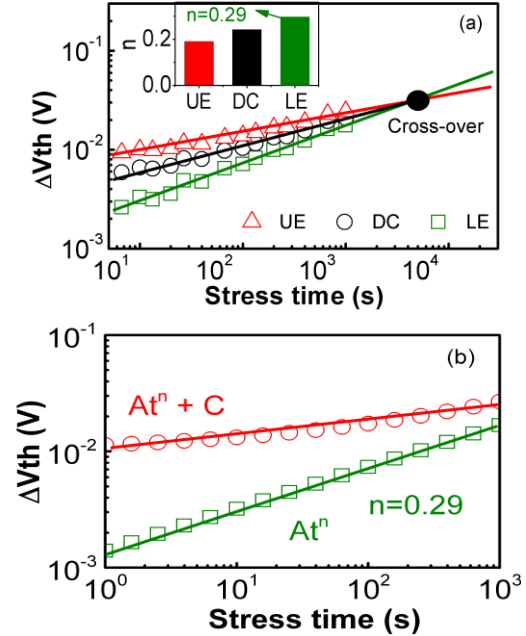


Fig. 2. (a) HCA kinetics for the mean of 40  $W=90\text{nm}$  devices. UE, DC, and LE have different ‘ $n$ ’ (inset). (b) Incorrect inclusion of an as-grown component, ‘C’, gives an apparent lower ‘ $n$ ’.

Given this uncertainty, the challenge is how to extract the time exponent,  $n$ , reliably for nano-devices. One effective method for suppressing the fluctuations in Fig. 1 is to use the mean value of multiple devices. Fig. 2(a) shows that smooth data are obtained for the UE, LE and DC, when the mean of 40 devices was used. The  $n$  extracted from these three, however, are different, with UE giving the lowest and LE having the highest  $n$ . This leads to the cross-over of LE from UE, when

extrapolating ahead, which is not physically meaningful, as the LE should never be higher than UE [19,20].

To investigate whether UE or LE should be used for extracting  $n$ , we examine their dependence on HCA. Fig. 3(a) clearly shows that LE increases progressively with HCA time, but the WDF=UE-LE remains the same. As a result, LE is caused by HCA, while WDF is not. WDF originates from the ‘as-grown’ defects in fresh devices [27,28]. To further support this, Fig. 3(b) shows that the mean of WDF for 40 devices is a constant against HCA time.

Since WDF is not caused by HCA, it should not be included when extracting the HCA time exponent [27]-[29]. In another word,  $n$  should be extracted from LE, rather than UE. UE gives a lower apparent  $n$ , because it contains as-grown traps. This can be demonstrated in Fig. 2(b): adding a constant to a power law leads to an apparent lower  $n$ .

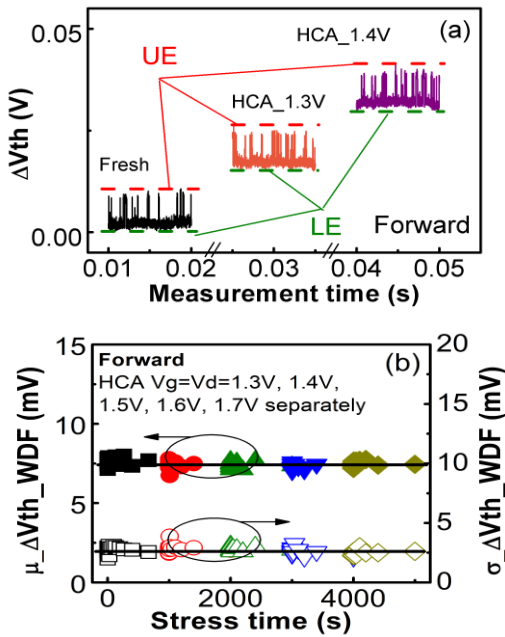


Fig. 3. (a) For  $L \times W = 27 \times 90 \text{ nm}$ , LE increases with HCA, but  $\text{WDF} = \text{UE} - \text{LE}$  does not. (b) The  $\mu_{\Delta V_{th\_WDF}}$  of 40 devices and its sigma do not increase with stress time.

### B. The contribution of PBTI

When stressed under  $V_g = V_d$ , the electrical field over the gate dielectric is not uniform. At the source end, the device suffers from positive bias temperature instability (PBTI) [12], while HCA dominates at the drain end for short channel. For long channel nMOSFETs (e.g.  $1.5 \mu\text{m}$ ), it is well known that HCA reduced for higher temperature [30]. Both HCA and PBTI, however, rise with temperature for modern CMOS nodes [12,23]. PBTI is process-dependent [31] and we now assess the relative contribution of PBTI to the aging for our devices under  $125^\circ\text{C}$ . Two test sequences were used in Fig. 4:

- (i) HCA(1<sup>st</sup> stress)-PBTI(2<sup>nd</sup> stress)-HCA(3<sup>rd</sup> stress);
- (ii) PBTI(1<sup>st</sup> stress)-HCA(2<sup>nd</sup> stress)-PBTI(3<sup>rd</sup> stress).

The same  $V_g$  were used for all stresses. A comparison of the two ‘1<sup>st</sup> stress’ in Fig. 4(a) shows that the HCA is clearly stronger than PBTI. The PBTI (2<sup>nd</sup> stress, the symbol ‘ $\Delta$ ’ in Fig.

4(a)) after the HCA (1<sup>st</sup> stress) only produces modest further aging. In Fig. 4(b), we remove the 2<sup>nd</sup> stress period, so that the HCA (3<sup>rd</sup> stress, ‘ $\blacksquare$ ’) is joined together with the HCA (1<sup>st</sup> stress, ‘ $\square$ ’). It can be seen that two HCA essentially follows the same kinetics, so that the impact of the PBTI (2<sup>nd</sup> stress) on the HCA kinetics is modest. As a result, the HCA kinetics reported in this work is dominated by the hot carrier aging process.

On the other hand, when the HCA (2<sup>nd</sup> stress, ‘ $\nabla$ ’) was applied after the PBTI (1<sup>st</sup> stress), Fig. 4(a) shows  $\Delta V_{th}$  rises substantially above the level extrapolated from the power law line of the PBTI (1<sup>st</sup> stress), confirming the dominance of HCA. When HCA (2<sup>nd</sup> stress) was removed and the PBTI (3<sup>rd</sup> stress) is joined with the PBTI (1<sup>st</sup> stress), Fig. 4(b) shows that the two PBTI do not follow the same kinetics.

It should be pointed out that, although HCA dominates the aging kinetics under our test conditions ( $V_g = V_d$  and channel length less than  $36 \text{ nm}$ ), the relative strength of PBTI against HCA will increase for longer channel and higher  $V_g/V_d$ .

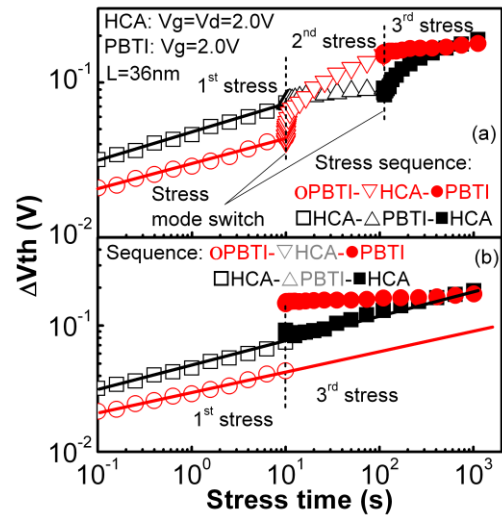


Fig. 4. (a) The black set of symbols follow the test sequence of HCA(1<sup>st</sup> stress), PBTI(2<sup>nd</sup> stress), and HCA(3<sup>rd</sup> stress). The red set of symbols follow the test sequence of PBTI(1<sup>st</sup> stress), HCA(2<sup>nd</sup> stress), and PBTI(3<sup>rd</sup> stress). (b) The 2<sup>nd</sup> stress periods were removed for both test sequences. The HCA kinetics is hardly affected by the preceding PBTI, but PBTI kinetics is substantially affected by the preceding HCA.

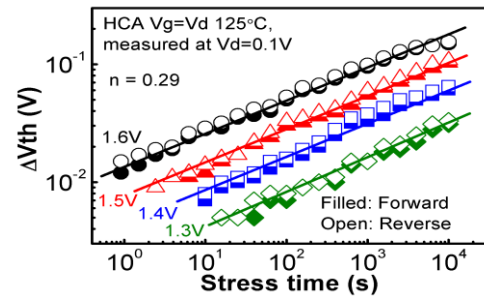


Fig. 5. Typical tests for extracting the voltage exponent repeats the tests under several different biases. The forward and reverse  $\Delta V_{th}$  measured under  $V_d = 0.1 \text{ V}$  agrees well here. The drain for stress and measurement is the same for the forward measurement, while the drain was swapped with the source after stress for the reverse measurement.

### C. Extraction of voltage exponent, $m$

The voltage exponent,  $m$ , is conventionally extracted by repeating the HCA under several (e.g. 4–6) different stress biases with one new device used for each bias, as shown in Fig. 5. This is acceptable for large devices where the DDV is negligible and only one test is needed for each bias. For nano-meter devices, however, multiple tests have to be carried out to take their considerable DDV into account [21,22]. The test time becomes costly and there is a need to reduce it.

A voltage-step-stress (VSS) technique has been proposed for negative bias temperature instability [32] that allows  $m$  being extracted from just one device and reduces the number of tests by ~80%. We investigate the applicability of VSS to HCA here, first on a large device (27×900 nm) and then on nano-devices.

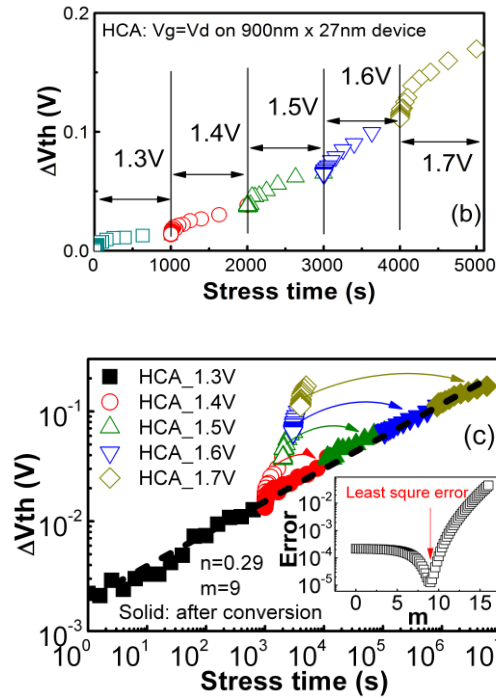
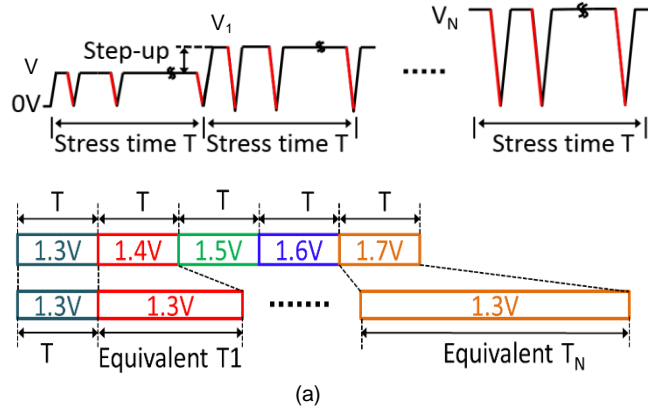


Fig. 6. Voltage-Step-Stress (VSS) technique for HCA. (a) One device was stressed for a time  $T$  and the stress  $V_g=V_d$  was then stepped up.  $\Delta V_{th}$  is plotted against linear (b) and log (c) stress time. The stress time under high bias is converted to an equivalent longer time at low bias by fitting the voltage exponent ‘ $m$ ’ (inset of (c)), based on eq. (2) in Table 1. The dashed line has  $n=0.29$  and  $m=9$ .

The principle of VSS is given in Fig. 6(a). The stress bias was applied for a given time and then raised in steps, so that different stress biases were applied to the same device. For the same stress time, HCA is higher under higher biases and typical results are given in Fig. 6(b). A HCA under a higher bias is equivalent to a HCA under a lower bias for a longer time, as illustrated in Figs. 6(a)&6(c) and this equivalent time can be evaluated by [32],

$$T_N = T(V_N/V)^{m/n}. \quad (2)$$

With  $n$  extracted from the 1<sup>st</sup> stress step,  $m$  can be extracted by converting the data in Fig. 6(b) to a power law in Fig. 6(c).  $m$  is fitted here by minimizing the least square error between the test data and the power law, as shown by the inset of Fig. 6(c).

We now apply the VSS technique to nano-devices. Although there is a large DDV, Fig. 7 shows that their mean value agrees well with that of a large device. As a result, the time and voltage exponents for the mean value of nano-devices can be extracted in the same way as that used for a large device: the  $n$  can again be extracted by fitting the first stress step and  $m$  is extracted by fitting the data at other voltage steps with the power law, as illustrated in Fig. 6(c).

### D. Verification of the extracted model

As the original mission for developing a model is to use it to make prediction, a model should be validated by verifying its prediction capability.

The test data under high stress biases (1.3 ~ 1.7 V) in Fig. 6 was used to extract the HCA model. We now verify its capability of predicting the HCA under low operation biases (0.9 ~ 1.2 V). Fig. 8 shows that the model prediction (lines) agree well with the mean test data. It should be emphasized that the test data in Fig. 8 themselves were not used for fitting the model parameters.

Based on the extracted model with  $n=0.29$  and  $m=9$ , Fig. 8 projects a mean  $\Delta V_{th\_LE}=18$  mV under an operation voltage of 0.9 V for 10 years. Adding the WDF, we have  $\Delta V_{th\_UE}=25.5$  mV. Once the mean,  $\mu$ , is predicted, the next task is to determine the standard deviation,  $\sigma$ .

It has been proposed that the time-dependent DDV follows a defect-centric model [21,22,33]. This model predicts that the relation between  $\mu$  and  $\sigma$  is [33],

$$\sigma = \sqrt{2\eta\mu}, \quad (3)$$

where  $\eta$  is the average impact of a trap on the device. Fig. 9(a) shows that HCA-induced DDV follows this relationship well. For a given predicted  $\mu$ , the corresponding  $\sigma$  can be determined from (3) fitted in Fig. 9(a). For example, for  $\mu=25.5$  mV, the corresponding  $\sigma$  is 13.0 mV. Fig. 9(b) shows that the statistical distribution of HCA-induced DDV agrees well with the defect-centric model.

E. Assessing the accuracy of statistical properties,  $\mu$  and  $\sigma$

As mentioned earlier, HCA tests are time consuming and only a limited number of DUTs can be used in practice for extracting the statistical properties: mean ( $\mu$ ) and standard deviation ( $\sigma$ ). For a given number of DUTs, the question is how accurate the extracted  $\mu$  and  $\sigma$  is. This information is missing from early works and we will develop a new method to address it next. The results in this section are from simulation.

The defect-centric model has been verified based on the test results of 92,000 DUTs from 4000 lots [22] and the HCA reported here also follows it well. We can use this model to assess the accuracy of  $\mu$  and  $\sigma$  extracted from a given number of DUTs by generating HCA in each hypothetical device, as detailed below.

To determine the statistical distribution of the defect-centric model, two parameters are needed: the average number of traps per device,  $N_t$ , and the average  $\Delta V_{th}$  induced by one trap,  $\eta$ . The  $\eta$  can be estimated from (3) and Fig. 9(a) and is  $\sim 3.4$  mV. With a typical lifetime criteria of 25 ~ 50 mV,  $N_t$  will be in the range of 7 ~ 15.

Once  $\eta$  and  $N_t$  is known, the number of traps in a hypothetical device,  $n_t$ , can be randomly generated by using Poisson distribution and the threshold voltage shift induced by a trap,  $\Delta V_{th,i}$ , can be obtained by using the exponential distribution, according to the defect-centric model [21,34]. The total  $\Delta V_{th}$  of this device is the sum of each-trap induced shift,

$$\Delta V_{th} = \sum_{i=1}^{n_t} \Delta V_{th,i}. \quad (4)$$

We will use  $N_t=7.5$  and  $\eta=3.4$  mV to demonstrate the method. The  $\Delta V_{th}$  for a hypothetical device, DUT1, is calculated according to (4). If we assume  $X$  devices have been used for evaluating  $\mu$  and  $\sigma$  in a test, i.e. the test 1 in Fig. 10, we can statistically calculate the  $\Delta V_{th}$  for these  $X$  devices. These  $X$   $\Delta V_{th}$  can then be used to calculate one  $\mu$  and one  $\sigma$ , as represented by a data point in Figs. 11(a)&11(b), respectively.

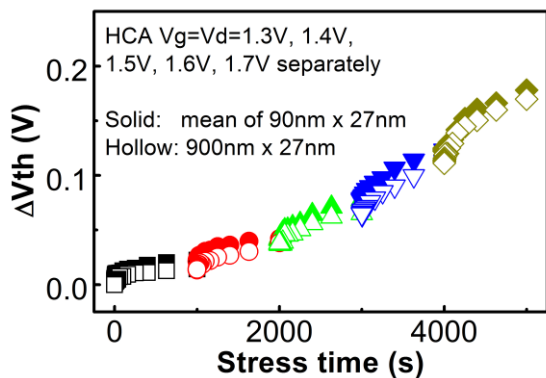


Fig. 7. The mean of 40 90x27nm devices agrees well with one 900x27nm for VSS stresses.

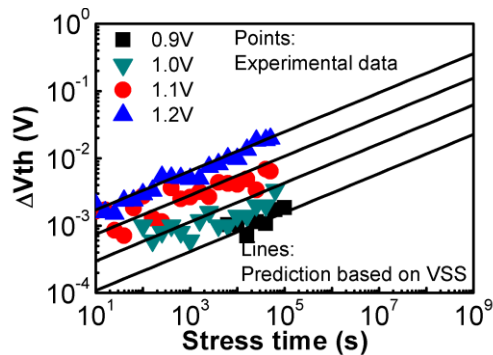


Fig. 8. A comparison of the model prediction with the test data for  $\Delta V_{th}$ . The model parameters in eq. (1) were extracted from VSS accelerated tests (see Fig. 7). The test data at lower voltages in this figure were not used for extracting the model parameters.

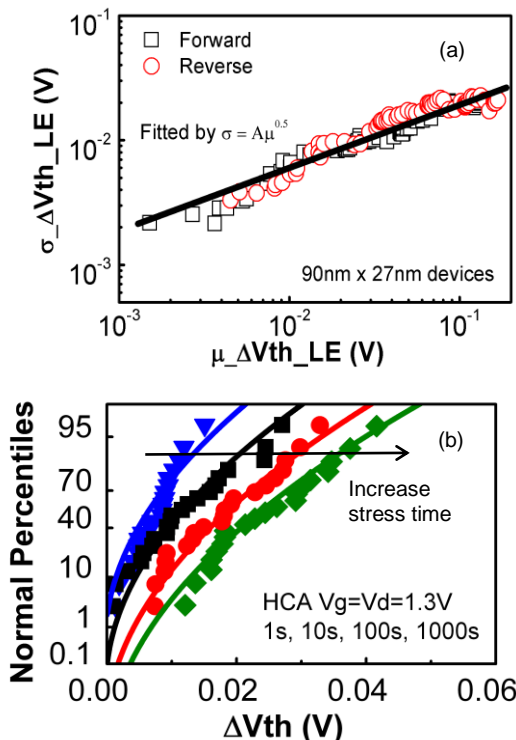


Fig. 9. Statistics of HVA-induced DDV. The lines are fitted with the defect-centric distribution. (a) Sigma versus mean. (b) Distribution after different stress time.

If another test engineer repeated the same test, i.e. the test 2 in Fig.10, a different group of  $X$  devices would be used, producing a different  $\mu$  and  $\sigma$  and give another data point in Fig. 11. Fig. 11 shows the statistical spread for 1000 tests, i.e.  $M=1000$  in Fig. 10, when  $X$  DUTs were used for each test. The  $X$  was varied between 20 and 1000. As expected, the spread becomes increasingly larger when a smaller number of DUTs were used for the test.

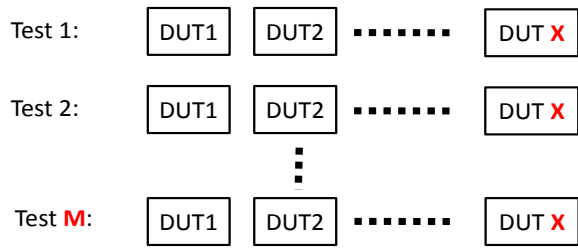


Fig. 10. An illustration of statistical tests: In a hypothetical Test 1, engineer 1 used X DUTs for extracting the  $\mu$  and  $\sigma$  of HCA. In test 2, engineer 2 also used X DUTs, but will obtain different  $\mu$  and  $\sigma$ , because a different set of devices were used.

The number of DUTs is not the only parameter controlling the accuracy of  $\mu$  and  $\sigma$ . Fig. 12 shows that for a given  $X=100$ , the spread reduces for higher  $N_t$ , because a higher number of traps per device averages out device variations to a certain extent.

This work used 40 DUTs and we now assess the accuracy of the evaluated  $\mu$  and  $\sigma$ . Fig. 13(a) shows that the evaluated  $\mu$  has an accuracy within  $\pm 14\%$  for  $N_t=10$ , with a 95% confidence. To assess the impact of  $N_t$ , Fig. 13(b) shows that the accuracy reaches  $\pm 6\%$  when  $N_t=40$ . If 1000 DUTs were used, the accuracy will improve to  $\pm 2.6\%$  for  $N_t=10$  and  $\pm 1.3\%$  for  $N_t=40$ .

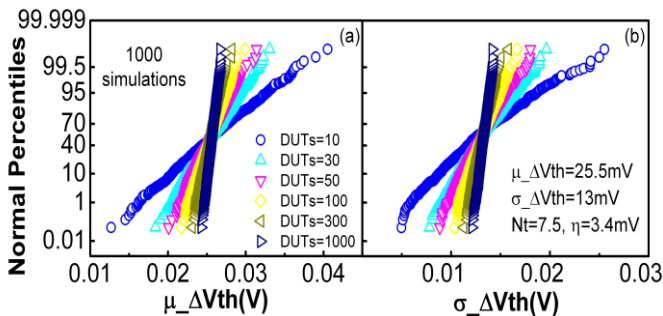


Fig. 11. The  $\mu$  (a) and  $\sigma$  (b) extracted for different DUTs (X in Fig. 12). For a given X, the tests were repeated 1000 times ( $M=1000$  in Fig. 12).

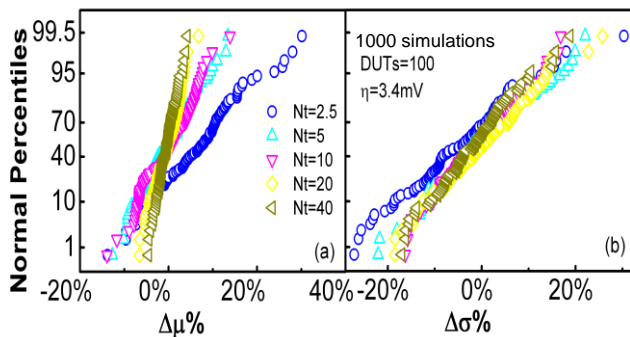


Fig. 12. The impact of the average number of traps,  $N_t$ , per DUT on the  $\mu$  (a) and  $\sigma$  (b) extracted for  $DUTs=100$  when the tests were repeated 1000 times ( $M=1000$  in Fig. 10).

The corresponding  $\sigma$  is given in Fig. 14. When  $DUTs=40$ , the evaluated  $\sigma$  has an accuracy within  $\pm 24\%$  for  $N_t=10$ , not as accurate as  $\mu$ . An increase of  $N_t$  to 40 only makes a modest

improvement to  $\pm 22\%$ . With 1000 DUTs, an accuracy of  $\pm 5\%$  can be achieved for  $N_t=10$ .

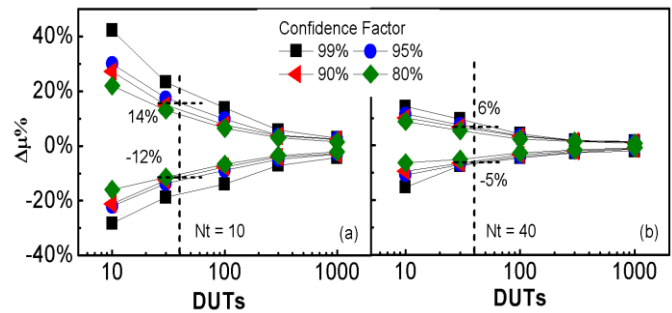


Fig. 13. The dependence of the accuracy of mean value,  $\mu$ , on the number of DUTs used in a test for  $N_t=10$  (a) and  $N_t=40$  (b). The accuracy with a 95% confidence is marked out for 40 devices.

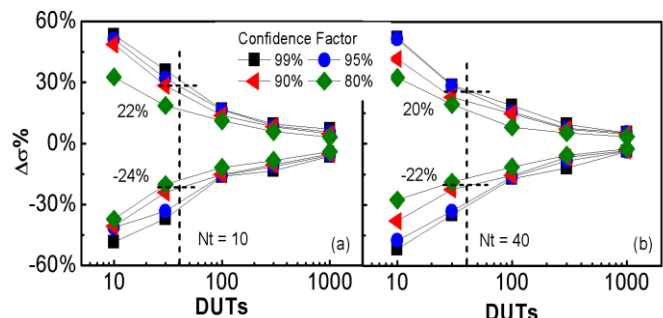


Fig. 14. The dependence of the accuracy of standard deviation,  $\sigma$ , on the number of DUTs used in a test for  $N_t=10$  (a) and  $N_t=40$  (b). The accuracy with a 95% confidence is marked out for 40 devices.

#### IV. CONCLUSION

This work investigates the key issues and provides solutions for characterizing the hot carrier aging of nano-devices. It is shown that the WDF is not caused by the HCA, so that they must be excluded, when extracting the HCA time-exponent. This can be achieved by using the lower envelope of WDF. The commercial source-and-measure unit measures a data point by taking the average within a period. This includes a part of WDF, resulting in an under-estimation of time exponent. The voltage exponent can be extracted by using the VSS technique, reducing the number of tests by  $\sim 80\%$ . HCA follows the defect-centric model well. Based on this model, the accuracy of the mean and standard deviation of device-to-device variation can be estimated for a given number of DUTs. For 40 DUTs with an average 10 traps per device, the accuracy for  $\mu$  and  $\sigma$  is  $\pm 14\%$  and  $\pm 24\%$ , respectively with a 95% confidence.

#### REFERENCES

- [1] C. Hu, S. C. Tam, F. C. Hsu, P. K. Ko, T. Y. Chan, and K. W. Terrill, "Hot-Electron-Induced MOSFET Degradation-Model, Monitor, and Improvement", *IEEE Trans. Electron Devices*, vol. ED-32, no. 2, pp. 375-385, 1985.
- [2] P. Heremans, R. Bellens, G. Groseneneken, and H. E. Maes, "Consistent model for the hot-carrier degradation in n-channel and p-channel MOSFET's," *IEEE Trans. Electron Devices*, vol. 35, no. 2, pp. 2194-2209, 1988.

- [3] J. F. Zhang and W. Eccleston, "Effects of high field injection on the hot carrier induced degradation of submicron pMOSFET's," *IEEE Trans. Electron Devices*, vol. 42, no.7, pp. 1269-1276, 1995.
- [4] A. Bravaix, Y. M. Randriamihaja, V. Huard, D. Angot, X. Federspiel, W. Arfaoui, P. Mora, F. Cacho, M. Saliva, C. Besset, S. Renard, D. Roy, E. Vincent, "Impact of the gate-stack change from 40nm node SiON to 28nm High-K Metal Gate on the Hot-Carrier and Bias Temperature damage", *IRPS 2013*, pp 2D.6.1-2D.6.9.
- [5] M. Duan, J. F. Zhang, A. Manut, Z. Ji, W. Zhang, A. Asenov, L. Gerrer, D. Reid, H. Razaidi, D. Vigar, V. Chandra, R. Aitken, B. Kaczer, and G. Groeseneken, "Hot carrier aging and its variation under use-bias: kinetics, prediction, impact on Vdd and SRAM", *IEDM 2015* pp. 547-550.
- [6] B. Kaczer, J. Franco, M. Cho, T. Grasser, Ph. J. Roussel, S. Tyaginov, M. Bina, Y. Wimmer, L. M. Procel, L. Trojman, F. Crupi, G. Pitner, V. Putcha, P. Weckx, E. Bury, Z. Ji, A. De Keersgieter, T. Chiarella, N. Horiguchi, G. Groeseneken, and A. Thean, "Origins and Implications of Increased Channel HotCarrier Variability in nFinFETs", *IRPS 2015*, pp 3B.5.1-3B.5.6.
- [7] N. H. Hsu, J. W. You, H. C. Ma, S. C. Lee, E. Chen, L. S. Huang, Y. C. Cheng, O. Cheng, I. C. Chen, "Intrinsic Hot-Carrier Degradation of nMOSFETs by Decoupling PBTI Component in 28nm High-K/Metal Gate Stacks", *IRPS 2012*, pp XT.13.1-XT.13.4.
- [8] J. H. Stathis, M. Wang, R. G. Southwick, E. Y. Wu, B. P. Linder, E. G. Liniger, G. Bonilla, H. Kothari, "Reliability Challenges for the 10nm Node and Beyond," *IEDM 2014*, p. 522-525.
- [9] G. T. Sasse, F. G. Kuper, and J. Schmitz, "MOSFET Degradation Under RF Stress," *IEEE Trans. Electron Devices*, vol. 55, no. 11, pp.3167-3174, 2008.
- [10] A. J. Scholten, D. Stephens, G. D. J. Smit, G. T. Sasse, and J. Bisschop, *IEEE Trans. Electron Devices*, vol. 58, no. 1, pp.1-8, 2011.
- [11] A. Bravaix, V. Huard, D. Goguenheim, and E. Vincent, "Hot-Carrier to Cold-Carrier Device Lifetime Modeling with Temperature for Low power 40nm Si-Bulk NMOS and PMOS FETs," *IEDM 2011*, p.622-625.
- [12] K. T. Lee, C. Y. Kang, O. S. Yoo, R. Choi, B. H. Lee, J. C. Lee, H. D. Lee, and Y. H. Jeong, "PBTI-Associated High-Temperature Hot Carrier Degradation of nMOSFETs With Metal-Gate/High-k Dielectrics", *IEEE Trans. Electron Devices*, vol. 29, no. 4, pp. 389-391, 2008.
- [13] C. Liu, K. T. Lee, S. Pae, and J. Park, "New Observations on Hot Carrier induced Dynamic Variation in Nano-scaled SiON/Poly, HK/MG and FinFET devices based on On-the-fly HCI Technique: The Role of Single Trap induced Degradation," *IEDM 2014*, p 836-839.
- [14] S. E. Rauch and G. La Rosa, "The energy-driven paradigm of NMOSFET Hot-carrier effects," *IEEE Trans. Device Mater. Rel.*, vol. 5, no. 4, pp. 701-705, 2005.
- [15] P. Magnone, F. Crupi, N. Wils, H. P. Tuinhout, and C. Fiegna, "Characterization and Modeling of Hot Carrier-Induced Variability in Subthreshold Region", *IEEE Trans. Electron Devices*, vol. 59, no. 8, pp. 2093-2099, 2012.
- [16] M. Bina, K. Rupp, S. Tyaginov, O. Triebel, and T. Grasser, "Modeling of Hot Carrier Degradation Using a Spherical Harmonics Expansion of the Bipolar Boltzmann Transport Equation", *IEDM 2012*, pp 713-716.
- [17] Y. M. Randriamihaja, A. Zaka, V. Huard, M. Rafik, D. Rideau, D. Roy, "Hot Carrier Degradation: From Defect Creation Modeling to Their Impact on NMOS Parameters", *IRPS 2012*, pp. XT.15.1-XT.15.4.
- [18] Failure Mechanisms and Models for Semiconductor Devices, JEDEC, Alexandria, VA, USA, 2011.
- [19] M. Duan, J. F. Zhang, Z. Ji, W. Zhang, B. Kaczer, T. Schram, R. Ritzenthaler, G. Groeseneken, and A. Asenov, "New analysis method for time-dependent device-to-device variation accounting for within-device fluctuation," *IEEE Trans. Electron Dev.*, vol. 60, no. 8, pp. 2505-2511, 2013.
- [20] M. Duan, J. F. Zhang, Z. Ji, W. Zhang, B. Kaczer, T. Schram, R. Ritzenthaler, G. Groeseneken, and A. Asenov, "Development of a Technique for Characterizing Bias Temperature Instability-Induced Device-to-Device Variation at SRAM-Relevant Conditions". *IEEE Trans. Electron Devices*, vol. 61, no. 9, pp. 3081-3089, 2014.
- [21] B. Kaczer, T. Grasser, P. J. Roussel, J. Franco, R. Degraeve, L. A. Ragnarsson, E. Simoen, G. Groeseneken, and H. Reisinger, "Origin of NBTI variability in deeply scaled pFETs," *IRPS 2010*, pp. 26-32.
- [22] C. Prasad, M. Agostinelli, J. Hicks, S. Ramey, C. Auth, K. Mistry, S. Natarajan, P. Packan, I. Post, S. Bodapati, M. Giles, S. Gupta, S. Mudanai, K. Kuhn "Bias Temperature Instability Variation on SiON/Poly, HK/MG and Trigate Architectures," *IRPS 2014*, pp. 6A.5.1-6A.5.7
- [23] A. Bravaix, C. Guerin, V. Huard, D. Roy, J. M. Roux, and E. Vincent, "Hot-Carrier acceleration factors for low power management in DC-AC stressed 40nm NMOS node at high temperature," *IRPS 2009*, pp. 531-548.
- [24] S. F. W. M. Hatta, Z. Ji, J. F. Zhang, M. Duan, W. Zhang, N. Soin, B. Kaczer, S. De Gendt, and G. Groeseneken, "Energy distribution of positive charges in gate dielectric: probing technique and impacts of different defects", *IEEE Trans. Electron Dev.*, vol. 60, no. 5, pp. 1745-1753, 2013.
- [25] A. Kerber and T. Nigam, "Correlation of BTI induced device parameter degradation and variation in scaled Metal Gate /High-k CMOS technologies," *IRPS 2014*, pp. 6A.6.1-6A.6.6.
- [26] M. Duan, J. F. Zhang, Z. Ji, J. G. Ma, W. Zhang, B. Kaczer, T. Schram, R. Ritzenthaler, G. Groeseneken, and A. Asenov, "Key issues and techniques for characterizing Time-dependent Device-to-Device Variation of SRAM," *IEDM 2013* pp. 774-777.
- [27] M. Duan, J. F. Zhang, Z. Ji, W. Zhang, B. Kaczer, T. Schram, R. Ritzenthaler, A. Thean, G. Groeseneken, and A. Asenov, "Time-dependent variation: A new defect-based prediction methodology," *VLSI Tech. Symp.* 2014, pp.74-75.
- [28] R. Gao, Z. Ji, S. M. Hatta, J. F. Zhang, J. Franco, B. Kaczer, W. Zhang, M. Duan, S. De Gendt, D. Linten, G. Groeseneken, J. Bi and M. Liu, "Predictive As-grown-Generation (A-G) model for BTI-induced device/circuit level variations in nanoscale technology nodes," *IEDM 2016*, pp. 778-781.
- [29] Z. Ji, S. F. W. M. Hatta, J. F. Zhang, J. G. Ma, W. Zhang, N. Soin, B. Kaczer, S. De Gendt, and G. Groeseneken, "Negative bias temperature instability lifetime prediction: Problems and solutions," *IEDM 2013*, pp. 413-416.
- [30] F.-C. Hsu, K.-Y. Chiu, "Temperature Dependence of Hot-Electron-Induced Degradation in MOSFET's", *IEEE Elec. Device Lett.*, vol. 5, no.5, pp. 148-150, 1984.
- [31] C. Z. Zhao, J. F. Zhang, M. B. Zahid, B. Govoreanu, G. Groeseneken, and S. De Gendt, "Determination of capture cross sections for as-grown electron traps in HfO<sub>2</sub>/HfSiO stacks," *J. Appl. Phys.*, 100, pp. Art. No.093716, 2006.
- [32] Z. Ji, J. F. Zhang, W. Zhang, X. Zhang, B. Kaczer, S. De Gendt, G. Groeseneken, P. Ren, R. Wang, and R. Huang, "A single device based Voltage Step Stress (VSS) Technique for fast reliability screening," *IRPS, 2014*, GD-2.1-GD-2.
- [33] L. M. Procel, F. Crupi, J. Franco, L. Trojman, and B. Kaczer, "Defect-Centric Distribution of Channel Hot Carrier Degradation in Nano-MOSFETs," *IEEE Electron. Dev. Lett.*, vol. 35, no. 12, pp. 1167-1169, Dec, 2014.